Physics of Plasmas

Measurement of the breathing mode oscillations in Hall thruster plasmas with a fast-diving triple Langmuir probe

Cite as: Phys. Plasmas **27**, 123502 (2020); https://doi.org/10.1063/5.0022928
Submitted: 24 July 2020 . Accepted: 02 November 2020 . Published Online: 03 December 2020

V. Giannetti, M. M. Saravia, and T. Andreussi

Physics of Plasmas ARTICLE scitation.org/journal/php

Measurement of the breathing mode oscillations in Hall thruster plasmas with a fast-diving triple Langmuir probe

Cite as: Phys. Plasmas **27**, 123502 (2020); doi: 10.1063/5.0022928
Submitted: 24 July 2020 · Accepted: 2 November 2020 ·
Published Online: 3 December 2020

V. Giannetti,[1,2,a] M. M. Saravia,[1,b] and T. Andreussi[1,2,c]

AFFILIATIONS

[1]Department of Civil and Industrial Engineering, University of Pisa, 56122 Pisa, Italy
[2]Space Propulsion Division, SITAEL S.p.A., 56121 Pisa, Italy

[a]Author to whom correspondence should be addressed: vittorio.giannetti@phd.unipi.it
[b]Electronic mail: manuel.saravia@ing.unipi.it
[c]Electronic mail: tommaso.andreussi@sitael.com

ABSTRACT

We developed a novel measurement apparatus and data processing technique that allow for the quantitative reconstruction of the effects of breathing mode oscillations on the main properties of the plasma in Hall thrusters. The approach is based on the use of a triple Langmuir probe mounted on a rapidly moving arm to scan the channel centerline and was validated in an experimental campaign on a 5 kW-class Hall thruster. The probe data were sampled at high frequency during its motion, and a Bayesian methodology was used to reliably infer the plasma properties from the instantaneous voltage and current measurements. In order to model the interaction of the electrodes with the plasma, a parameterization of the Laframboise sheath solution was used. Data were collected continuously during the probe motion from the plume up to the near-anode region of the thruster, allowing for the reconstruction of the salient features of the plasma oscillations as a function of axial location. A time–frequency analysis of the measured plasma properties based on wavelets was then performed to gain insight into the evolution and phase shift of the oscillations over the investigated plasma domain. The developed diagnostic method can provide quantitative information on the instantaneous value of plasma density, electron temperature, and plasma potential along the thruster centerline with good spatial resolution and has proved to be a valid approach to investigate breathing mode oscillations in Hall thruster plasmas.

I. INTRODUCTION

In recent years, Hall thrusters have gained momentum as the most promising and widely adopted electric propulsion technology for space applications. This is due to their intrinsic high efficiency, high thrust-to-power ratio, and robust design. A Hall thruster is based on four core elements: an annular discharge channel, typically made of ceramic materials, a magnetic circuit, and two electrodes, i.e., the anode and cathode. The anode is located inside the discharge channel and neutral propellant, typically xenon, is injected through it. The cathode is positioned outside of the channel and it uses thermionic emission of electrons to sustain the discharge and neutralize the outbound ion beam. During operation, the anode is biased a few hundred volts with respect to the cathode and, thus, the generated electrons are attracted toward the channel. Close to the exit section of the discharge channel, the magnetic circuit generates a quasi-radial magnetic field that hinders the axial motion of the electrons. The localized decrease in electron mobility also implies the generation of a strong axial electric field in the same region. The thruster cross field configuration induces an $E \times B$ motion of the electrons in the azimuthal direction. When the neutral atoms injected through the anode reach the region of high azimuthal electron current, they are ionized by electron impact. The magnetic field is tuned to avoid magnetization of the ions, that are accelerated outward by the potential drop, generating thrust. Finally, a second population of electrons is emitted by the cathode to neutralize the beam and preserve the charge balance of the system.[1]

The plasma generated inside Hall thrusters exhibits a number of unsteady modes, the characteristics of which vary greatly with the geometry, magnetic field topology, and operating conditions of the thruster.[2–4] One of the most relevant oscillatory modes, found ubiquitously in Hall thrusters, is the so-called breathing mode. This is

recognized as a macroscopic axial ionization instability that manifests itself as a relatively low frequency (10–30 kHz) high amplitude oscillation of the discharge current and of the plasma parameters. The existence of this longitudinal mode was first reported in the mid 1970s[5] and it was observed on most, if not all, thruster models. Breathing mode oscillations were investigated numerically since the advent of plasma simulations in the field,[6,7] and more recent advancements in the numerical description of Hall thruster discharges[8–11] aided in obtaining a greater understanding of the origin and characteristics of this phenomenon. An intuitive understanding of the physical mechanism at the core of breathing mode oscillations can be traced back to a periodic ionization and replenishment of neutrals in the channel and the consequent periodic expulsion of ions. Nevertheless, the impact of breathing mode oscillations on the thruster operation and performance is still a subject of debate. This is due to its complex interaction with other oscillatory modes that generate anomalous diffusion of the electrons through the magnetic field[1] and to the difficulties in gathering reliable experimental data in the near field of Hall thrusters.

As a matter of fact, performing measurements inside the channel and in the near plume of Hall thrusters is a challenging task for both intrusive and non-intrusive diagnostic systems, even more so when high frequency data need to be collected to reconstruct oscillatory modes. This is due to the harsh plasma environment the probes are subject to, posing strict constraints on the probe materials, design, and on the residence time in the high plasma temperature region. Moreover, intrusive probes can significantly perturb the plasma flow and, thus, special care must be put in the diagnostic system design and data interpretation. Finally, the thruster annular geometry and complex test setup pose limitations to the use of optical systems. Fast-diving probes were first used in the late 1990s to investigate time-averaged plasma properties inside a Hall thruster.[12] Several other iterations of this method are found in the literature using emissive probes, as well as single and triple Langmuir probes.[13–18] The perturbation of the plasma properties introduced by the probe insertion poses concerns on the interpretation of the data, especially inside the channel and where a strong azimuthal electron current is present. Several authors have studied the magnitude of the perturbation in order to improve the reliability of the gathered data. Haas *et al.*[12] describe how a reduction in the residence time of the probe in the high temperature region of the plasma can significantly reduce the perturbation by minimizing material ablation. Nevertheless, a certain degree of perturbation still remains and the thruster global parameters show a sharp transition during the probe insertion. Jorns *et al.* also discuss this phenomenon in Ref. 17, where they highlight how the plasma properties profiles shift downstream by 15%–20% of the channel length during the probe insertion. Non-intrusive optical methods, such as Thompson scattering[19] or laser induced fluorescence (LIF) spectroscopy,[20–23] are alternatives to fast-diving probes to gather information on the plasma properties in the near field of Hall thrusters. While of great interest, these diagnostic systems can present signal to noise interpretation issues and typically require very complex and expensive test setups which hinder their wide scale use. Multiple research groups have adopted some of these experimental techniques to investigate the longitudinal temporal evolution of the plasma properties in Hall thrusters during breathing mode cycles. A relevant example of the use of invasive probes is the work of Lobbia and Gallimore[24–27] where a single Langmuir probe (with a secondary noise compensating null probe) was used at multiple fixed locations in the thruster plume and rapidly biased to obtain plasma properties measurements on a 2D grid. Since single probes require time to be biased, the investigation only considered the far plume where the probe could survive indefinitely.

In the present research, we used a fast-moving triple Langmuir probe[14] to quantitatively reconstruct the oscillations in the plasma density, electron temperature, and plasma potential along the channel centerline from the plume up to the near anode region. The use of a triple probe allows to gather instantaneous measurements of the plasma properties without the need for voltage sweeps. The underlying assumption is that the electrons in the plasma follow a non-drifting Maxwellian velocity distribution function. This is considered acceptable to a first order, particularly in the plume, where the electron drift velocity is much lower than the thermal velocity. Moreover, the impact of the drift velocity component for the electrons is mitigated by the introduction of correction parameters in the particle collection model. The combination of the triple probe setup with the used data analysis method allowed us to measure the oscillations close to the channel exit and even inside the discharge channel by minimizing the residence time of the probe in the high temperature region. Moreover, since the characteristic times of the motion of the probe are orders of magnitude higher than the characteristic times of the breathing mode, a local description of the plasma oscillations can be recovered by measuring the plasma properties during the probe motion. The data gathered by the probe were sampled at 5 MHz during its motion but the bandwidth of the amplifiers used within the data acquisition system limited the investigations to 120 kHz, sufficient for capturing breathing mode oscillations. The data were then processed by defining a moving window of samples on which a Bayesian regression analysis was performed, as detailed in Ref. 14. This allowed to reconstruct the most likely plasma state as a function of axial location based on the instantaneous measurements, while keeping track of the uncertainty in the estimations. Furthermore, a time-frequency wavelet analysis of the complete dataset was performed to highlight the most salient characteristics of the longitudinal oscillations as a function of axial location. This analysis also shows the realization of the breathing mode, observed through discharge current oscillations, as a coherent wave in the plasma properties across the plasma domain. Finally, a technique for spatiotemporal data merging was developed and used to visualize the effect of the breathing cycles on the plasma properties simultaneously on the whole investigated domain.

In this paper, we describe this novel method for the measurement of the plasma oscillations in Hall thrusters and demonstrate its effectiveness on a set of measurements gathered on the HT5k, a 5 kW-class Hall thruster developed at SITAEL.[28] Section II provides an overview of the test setup, including probe design, moving arm, test item, test facility, and high frequency data acquisition system. In Sec. III, the post-processing logic is presented, including probe theory, Bayesian inference algorithm, time–frequency analysis, and spatiotemporal data merging technique. Section IV shows the results of the processing technique applied on the test data gathered on the HT5k experimental campaign, highlighting the most salient characteristics of the observed plasma oscillations. Finally, Sec. V summarizes the conclusions of the present research.

II. HIGH-SPEED TRIPLE PROBE DIAGNOSTIC SYSTEM

The hardware test setup used for this measurement technique was already presented and described in detail by the authors in

previous publications.[13–15] Therefore, only its most important features are hereby summarized, with the addition of the description of the high frequency data acquisition system.

A. Probe design and fast-diving mechanism

The triple Langmuir probe is a plasma diagnostic device constituted by three electrodes that allow for the instantaneous measurement of the plasma density n, potential V_{gp}, and electron temperature T_e.[14,29] The three electrodes are commonly denominated float (F), common (C), and bias (B). The F electrode is left floating, while a potential difference is applied between C and B. In the present study, a bias voltage applied between electrodes B and C of 30 V was selected. This value is considered sufficiently high to provide good accuracy of the measurements in the temperature range of interest but sufficiently low to avoid test setup complications and safety concerns. During the probe operation, the current flowing between B and C is collected (I_{BC}), together with the voltage between F and C (V_{FC}) and the voltage between the ground and C (V_{gC}). The three measures, coupled with a model of the plasma interaction with the electrodes, are sufficient to reconstruct the local values of plasma density, potential, and electron temperature. A schematic representation of the device is reported in Fig. 1 together with the physical description of the probe used in the present study. The three electrodes were derived from 75% tungsten, 25% rhenium alloy wires with a diameter of 0.178 mm and installed inside a 1/8 in. alumina insulating tube. While the high secondary electron emission of alumina would imply a higher perturbative effect in the high temperature plasma regions, this ceramic was selected due to its high mechanical strength and availability in the required format. In order to avoid undesired interaction between the electrodes, a minimum distance of 2 mm was established. Considering that the Debye length of the probed plasma is always smaller than 0.1 mm, the separation distance of 2 mm allows to always have more than 20 Debye lengths separating the tips and was considered as the best trade-off between minimizing electrode interaction and maximizing the probe spatial resolution. Furthermore, each electrode was 2.6 ± 0.1 mm long to allow neglecting tip effects.

The probe was installed on a mechanical arm, shown in Fig. 2 (top), that supported the probe and allowed for its rapid insertion and retraction from the plasma domain. During its motion, the arm and, thus, the probe performed a circular trajectory with a radius of 350 mm. The acquisition was only performed in the final 0.27 rad arc of the probe motion in the near plume and channel region of the thruster. Considering the 350 mm arm length, this implied a maximum deviation from the channel centerline of 0.2 mm inside the channel and 9.5 mm in the plume. In order to minimize the exposure of the probe to the high plasma density and temperature environment, the diagnostic system was kept in a parking position when non-operational, far from the plasma domain. When measurements were required, a high-speed magnetic actuator moved the arm in and out of

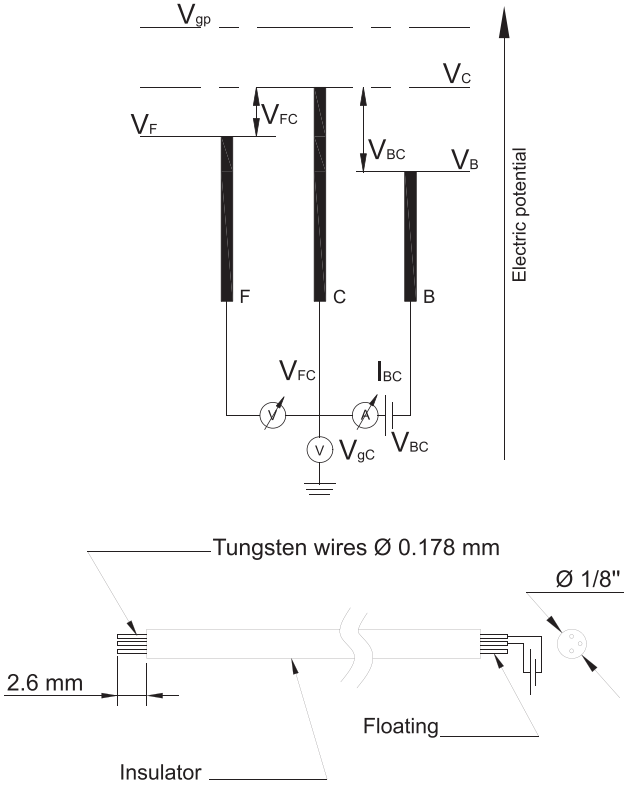

FIG. 1. (Top) schematic depiction of a triple Langmuir probe; (bottom) constructive scheme of the probe used in the present study. Reproduced with permission from Saravia *et al.*, Rev. Sci. Instrum. **90**, 023502 (2019). Copyright 2019 AIP Publishing.[14]

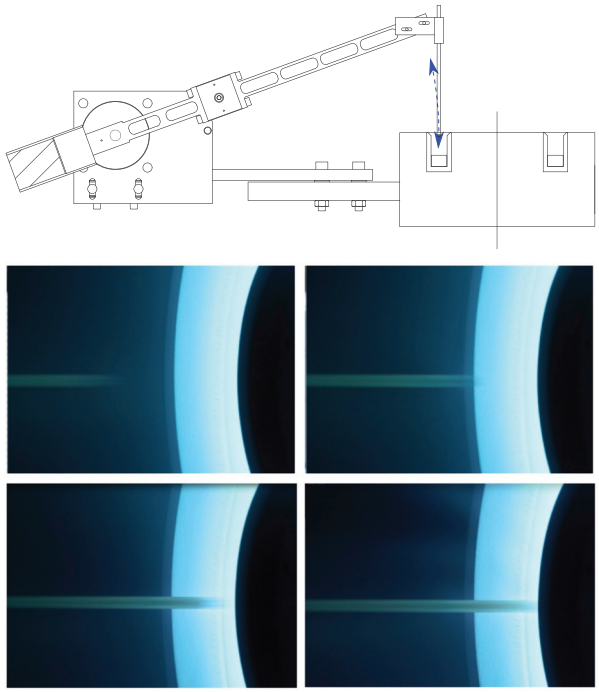

FIG. 2. (Top) articulated arm during triple probe insertion. The blue dotted line represents the acquisition region of the trajectory; (bottom) successive video frames captured during probe insertion in the HT5k thruster during operation. Reproduced with permission from Saravia *et al.*, Rev. Sci. Instrum. **90**, 023502 (2019). Copyright 2019 AIP Publishing.[14]

the acquisition region in 200 ms. The position of the probe along its motion was recorded with an encoder, ensuring a resolution of the probe position of 0.3 mm. Figure 2 (bottom) shows successive images of the probe being inserted in the thruster channel. Each of the still frames was taken 0.02 s apart.

B. Test item and test setup

The effectiveness of the diagnostic system presented in this work was tested by measuring the longitudinal oscillatory plasma modes of a 5 kW-class Hall thruster. Particularly, the second development model (DM2) of SITAEL's HT5k[28] in the M1 magnetic configuration was used (for further details refer to Ref. 13). All elements of the thruster magnetic circuit are made of soft magnetic alloy and, when magnetized by coils, allow producing an almost radial magnetic field at the exit plane of the thruster accelerating channel. The HT5k was equipped with the HC20 high-current hollow cathode, also developed by SITAEL. Figure 3 shows the HT5k DM2 thruster firing and highlights three axial positions that will be investigated in greater depth in the following: z_1 located just 2 mm downstream of the channel exit section, z_2, 20 mm downstream of the channel exit section, representative of near-plume conditions, and z_c, 60 mm downstream of the exit section. As shown in Fig. 3, z_c was selected for detailed investigation because it corresponds to the intersection of the probe trajectory with the first magnetic field line that reaches the cathode near-field plasma. Considering the magnetized dynamics of the electrons emitted from the cathode and the presence of a bright plasma bridge along that particular magnetic field line, the point z_c was considered to be representative of the thruster-cathode coupling region. Observe that Fig. 3 is only intended for a qualitative understanding of the relevant features, exploiting the expected axial symmetry of the plasma, but the plane containing the probe trajectory is actually orthogonal to the axial plane intercepting the cathode.

The test campaign was carried out in SITAEL's IV4 vacuum facility.[30] IV4 is a nonmagnetic stainless-steel chamber with a diameter of 2 m and a length of 4.2 m. The facility is equipped with an oil-free pumping system constituted by a combination of cold heads, turbomolecular pumps, and cryogenic pumps with a pumping speed of 70 000 l/s for xenon. The typical base pressure of the system is below 10^{-7} mbar ($<7.5 \times 10^{-8}$ Torr), and during the thruster operation, the pressure was always measured to be below 10^{-4} mbar ($<7.5 \times 10^{-5}$ Torr).

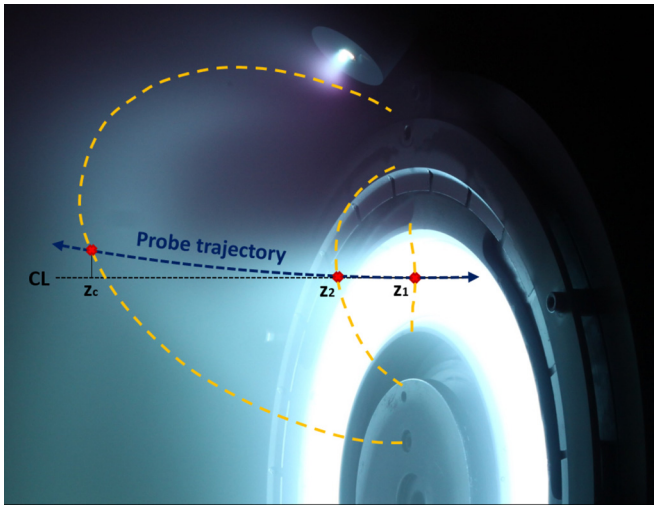

FIG. 3. HT5k DM2 thruster firing with HC20 visible at the top with relevant magnetic field lines and probe trajectory highlighted.

To validate the diagnostic method, a single low-power operating condition for the thruster was selected, with the operating parameters detailed in Table I. This specific condition was selected to reduce the power deposited on the probe and because it showed very clearly the breathing mode dynamics.

C. Data acquisition system

In order to extract the relevant probe signals, the three electrodes were connected to an analogue electronic box designed for high speed data acquisition. A schematic of the system is reported in Fig. 4. It is worth noting that this data acquisition system employed analog devices' AD215 120 kHz bandwidth, low distortion, isolation amplifiers. These items effectively limit the maximum frequency of the signal features to be investigated. Nevertheless, breathing mode oscillations (and their potential first harmonics) typically have much lower characteristic frequencies and, thus, the developed data acquisition system is suited for their investigation. The acquisition of the fast Langmuir probe signals from the electronic box output was performed using a Tektronix DPO 4104 digital oscilloscope with a sampling rate of 5 MHz. A photocell activated by the passage of the mechanical arm triggered the data storage. Additionally, the thruster discharge current was sampled by the oscilloscope simultaneously with the probe signals using a LEM LA25-NP current probe.

III. POST-PROCESSING AND BAYESIAN RECONSTRUCTION OF PLASMA OSCILLATIONS

This section presents the data analysis methodology used to calculate the plasma parameters from the measured signals. Additionally, the wavelet-based technique used to perform a time–frequency analysis of the signals is described. Finally, the procedure for spatiotemporal data merging developed to reconstruct the plasma global modes is presented.

A. Analysis methodology of triple Langmuir probe data

The data gathered during the experimental campaign consist of the time series of the potential difference between electrodes F and C, the potential of the C electrode with respect to the ground, the current flowing between the B and C electrodes, and the position of the probe tip. The methodology used to analyze the data, detailed by Saravia *et al.* in Ref. 14, consists of a Bayesian inference of the plasma properties (n, T_e, and V_{gp}) from the experimental measurements (V_{gC}, V_{FC},

TABLE I. HT5k operating condition selected for investigation.

AMFR[a] (mg/s)	Voltage (V)	Current (A)	Power (W)
8	300	8.65[b]	2595[b]

[a]Anode mass flow rate.
[b]Time-averaged value.

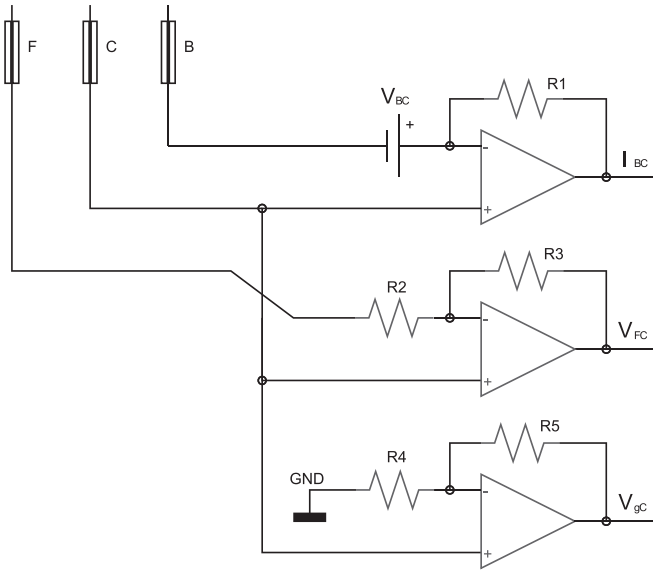

FIG. 4. Schematics of the analogue electronic box used to extract the probe signals.

and I_{BC}). Additionally, the implemented method considers a correction to take into account the mutual interaction between the different probe electrodes. It is worth remarking that in the analysis presented in Ref. 14, the data were arranged as a function of position to allow the merging of data from several sets of measurements. In the present research, the method is applied on time series of the measured parameters, with correction parameters calculated as a function of position.

Bayesian data analysis is a branch of Bayesian probability theory (BPT), which allows to combine measured data with physical models to perform inferences of the underlying state of a system, while consistently keeping track of the uncertainties. The following is a brief description of the main features of the Bayesian approach, relevant for the present research, we recommend the reader to read Refs. 31 and 32 for a more complete discussion on the topic.

BPT associates a probability distribution to the "state of knowledge" of a given parameter, which can be updated when new measurements are considered using the Bayes rule, reported in Eq. (1). When dealing with multiple parameters, the knowledge is represented by the joint probability distribution of all parameters, on which the marginalization rule can be applied to obtain the distribution of the parameters of interest

$$p(\mathbf{\Theta}|\mathbf{D},I) = \frac{p(\mathbf{D}|\mathbf{\Theta},I)\cdot p(\mathbf{\Theta}|I)}{p(\mathbf{D}|I)}. \tag{1}$$

The vector $\mathbf{\Theta}$ contains the sought plasma properties and the two correction parameters δV_1 and δV_2 to account for electrodes' mutual interactions[14]

$$\mathbf{\Theta} = \begin{bmatrix} T_e \\ n \\ V_{gp} \\ \delta V_1 \\ \delta V_2 \end{bmatrix} \tag{2}$$

while $\mathbf{D}$ represents the mean values of the experimental measurements at a given time t

$$\mathbf{D} = \begin{bmatrix} V_{gC} \\ V_{FC} \\ I_{BC} \end{bmatrix}. \tag{3}$$

Finally, I represents all the relevant background information available, such as the nature of the variables and how they relate to each other. In the following, we describe each term of the Bayes rule. The prior knowledge, $p(\mathbf{\Theta}|I)$, is the probability distribution of $\mathbf{\Theta}$ before the data are analyzed. In the present analysis, wide constant prior distributions are initially assigned to the plasma parameters to represent the lack of knowledge of the specific values, defining only a range within which the values are present: 0.01 to 100 eV for T_e, 10^{15} to 10^{20} m^{-3} for n, and -25 to 330 V for V_{gp}. The calculation of the prior probabilities for the correction factors is detailed later in the present paragraph.

The term $p(\mathbf{D}|\mathbf{\Theta},I)$ is the likelihood of the experimental data given a certain value of $\mathbf{\Theta}$, and relates both $\mathbf{D}$ and $\mathbf{\Theta}$ through a given function, in this case a multivariate Gaussian distribution

$$p(\mathbf{D}|\mathbf{\Theta},I) = \frac{\exp\left(-\frac{1}{2}(\mathbf{D}-\mathbf{Y})^T\mathbf{\Sigma}^{-1}(\mathbf{D}-\mathbf{Y})\right)}{\sqrt{(2\pi)^N|\mathbf{\Sigma}|}}, \tag{4}$$

where N is the number of variables ($N=5$ in this case), $\mathbf{\Sigma}$ is the covariance matrix of the data at a given time, and $\mathbf{Y}$ is a forward physical model that calculates the theoretical measured values as a function of a given combination of plasma parameters

$$\mathbf{Y} = \begin{bmatrix} V_{gC} \\ V_{FC} \\ I_{BC} \end{bmatrix} = f\left(\begin{bmatrix} T_e \\ n \\ V_{gp} \\ \delta V_1 \\ \delta V_2 \end{bmatrix}\right) = f(\mathbf{\Theta}). \tag{5}$$

The physical model portrays the particle collection process in the probe electrodes. It is based on the parameterization published by Mausbach[33] of the Laframboise solution of the plasma sheath,[34] which considers sheath expansion effects. According to Ref. 33, the current collected by an electrode immersed in a plasma and biased to a generic potential V_{pr} with respect to the ground is

$$I(V_{pr},T_e,n,V_{gp}) = Aen\sqrt{\frac{eT_e}{2\pi m_e}}\left[\exp\left(\frac{V_{pr}-V_{gp}}{T_e}\right) - \sqrt{\frac{m_e}{m_i}}a\left(b-\frac{V_{pr}-V_{gp}}{T_e}\right)^c\right], \tag{6}$$

where A is the exposed area of the electrode, n, T_e, and V_{gp} are the local plasma properties, e is the electron charge, m_e is the electron mass, and m_i is the ion mass. The parameters a, b, and c are functions of the ratio between the electrode radius r and the local Debye length $\lambda_D = \sqrt{\frac{\varepsilon_0 T_e}{en_e}}$, and correct the model to account for the finite dimensions of the electrode and for sheath expansion effects. These parameters are valid for the ion saturation region under the assumption of cold ions. Upon

setting up Eq. (6) for each of the three electrodes of the Langmuir probe, and after rearranging the terms, the resulting implemented model consists of the following expressions, relating the current collected by the electrodes B, C, and F (for a detailed description of the model, see Ref. 14):

$$I_B = I(V_{gC} - V_{BC}, T_e, n, V_{gp}) = -I_{BC}, \tag{7}$$

$$I_F = I\left(V_{gC} - V_{FC}, T_e, n, V_{gp} + \delta V_k\right) = 0, \tag{8}$$

$$I_C = I\left(V_{gC}, T_e, n, V_{gp} + \delta V_j\right) = I_{BC}. \tag{9}$$

Observe how the δV_j and δV_k parameters correct the local plasma potential sensed by a given electrode depending on their physical arrangement on the probe tip. The subscripts j and k indicate the relative position of the electrodes. A value of 1 for either j or k indicates that the respective electrode is in the position screened from the electron azimuthal current, whereas the value 2 indicates the corresponding electrode is not screened. The two electrodes arrangements considered for the correction take the values $j=1$ and $k=2$ for the case with electrode C in the screened position, and $j=2$ and $k=1$ for the case with electrode F in the screened position. The system of Eqs. (7)–(9) is solved for V_{gC}, V_{FC}, and I_{BC} for a given value of the plasma properties and of the potential inhomogeneities correction terms.

The posterior probability distribution $p(\mathbf{\Theta}|\mathbf{D}, I)$ is the resulting updated knowledge on our variable $\mathbf{\Theta}$ after the data $\mathbf{D}$ have been considered, together with the prior and the background information I. Finally, the evidence $p(\mathbf{D}|I)$ is the probability of observing the data under consideration. The evidence allows comparing the quality of the inferred values obtained using different models or hypotheses (also called model comparison problem[32]) but in parameter estimation problems as the present one, it is only used as a normalization value.

As stated before, in the case of dealing with a joint probability distribution, the marginalization rule, seen in Eq. (10), allows to integrate over the full range of a certain variable to calculate the probability distribution of the remaining parameters regardless of the value of the marginalized variable[31,32]

$$p(\theta_1|D, I) = \int_{-\infty}^{+\infty} p(\theta_1, \theta_2|D, I) d\theta_2. \tag{10}$$

An interesting feature which results from the marginalization rule is that it allows to include nuisance parameters within the model, i.e., variables for which the result is usually not of interest but are necessary to obtain a solution to the problem. This is done by assuming a probability distribution for the new parameter and then marginalizing over its full range to have a result that does not depend on the marginalized parameter.[31] In the present work, the correction parameters δV_1 and δV_2 are treated as nuisance parameters, as they are necessary to properly take into account the interaction effects within the model, but are not part of the desired solution.

The joint posterior probability distribution is the full representation of the current knowledge of a certain system. This representation can be simplified by marginalizing each parameter separately to obtain a probability distribution for each one of them. When possible, this distribution can be further summarized by defining a confidence interval or by calculating statistics such as the mean or the most likely value, together with the related error bars.

The inference process uses an implementation of the nested sampling algorithm[32,35] to carry out the Bayesian regression. This algorithm samples the prior probability domain of the plasma properties and the correction parameters, then it solves a forward model of the particle collection process for the sampled points. Then these results are compared to the measured data using a likelihood function and calculates the *a posteriori* probability. This process is repeated until the regions of higher probability within the domain are identified and the posterior joint probability distribution of all the parameters is obtained. Finally, this joint probability is marginalized to obtain the resulting distribution for each parameter. The nested sampling parameters were set to 70 live points, three Monte Carlo iterations and a tolerance of 0.001. A sensitivity analysis used to select the number of live points is described in the Appendix.

Unlike the cases analyzed in Refs. 14 and 15, in which the distributions were obtained as a function of axial position, the present analysis studies the time evolution of the plasma properties. The data were aggregated calculating the average and the covariance matrix of all the measured parameters for subsets of 20 time steps, resulting in a downsampling from 500 000 samples at 5 MHz to 25 000 at 250 kHz. Figure 5 shows an example of the raw measurements and the

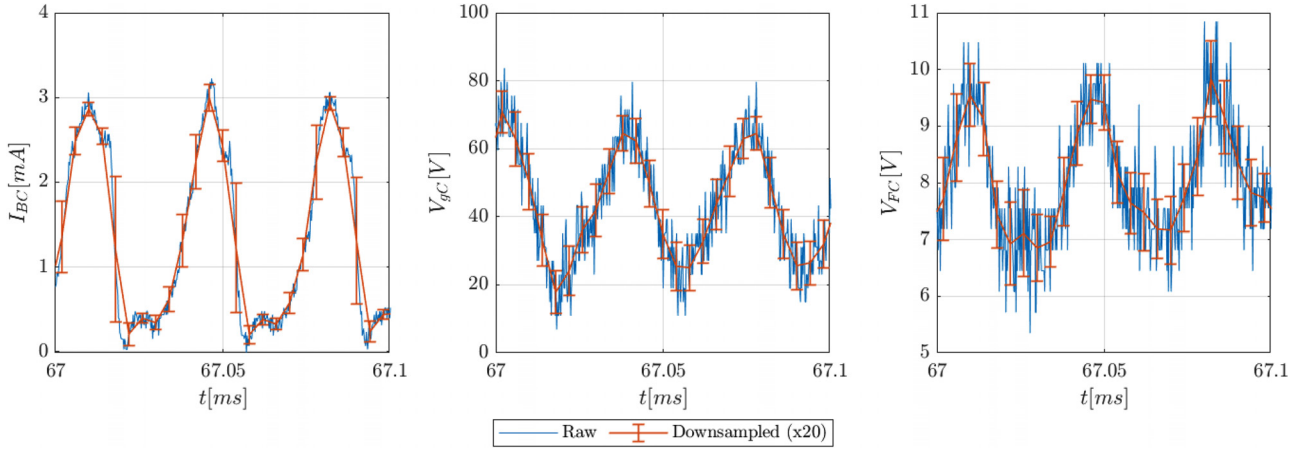

FIG. 5. Raw triple Langmuir probe data and downsampled data with 1-σ standard deviation error bars for position z_1.

downsampled data and their standard deviations for 0.1 ms in the z_1 position. It can be seen that the current has a rather clean signal, while the voltage signals have a larger noise component.

Using the downsampled data, the plasma parameters were calculated using the procedure described in the previous paragraphs. Figure 6 presents the results corresponding to the raw data from Fig. 5. As the results show, the uncertainty in the density is smaller, as the model has a predominantly linear dependence on this parameter (except for a sheath thickness correction that depends weakly on the Debye length[33]), while the results are more uncertain for the plasma potential and electron temperature, on which the model has an exponential dependence.

Reference 14 analyzes the effect of mutual perturbation between the probe electrodes and concludes that the interaction is caused by the screening of the azimuthally flowing electron currents, affecting the local potential sensed by the different electrodes. As a consequence, Saravia *et al.*[14] took advantage of the capability of Bayesian data analysis to combine different datasets[32] to propose a way of quantifying this mutual potential perturbation effect and to correct the inferred values of the plasma properties (through the introduction of the two correction parameters δV_1 and δV_2 in the vector $\boldsymbol{\Theta}$). Saravia *et al.* dealt with steady spatial distributions of the plasma properties, which allowed to merge the data from different sets of measurements considering their axial position to perform the parameter inference. The same approach is not easily implemented for the unsteady analysis subject of the present research, given that the phase of the oscillations of the plasma properties in a certain position will differ for different probe insertion cycles. Consequently, we assumed that the mutual perturbation was a steady phenomenon, only function of the axial position of the probe, considering the time-variation of the correction parameters as a second order effect.

The modified analysis starts by considering datasets belonging to the same operative point in which the bias applied between the B and C electrodes is taken to zero, considering two probe configurations with different electrodes arrangements. Under a steady and homogeneous plasma condition having short-circuited the two tips would result in a null-current flowing between the electrodes, regardless of the probe arrangement. Nevertheless, a net current is observed, and this effect is used to put in evidence the plasma local inhomogeneities. By performing the Bayesian inversion combining the datasets for both electrodes arrangements, the local plasma properties are obtained. It is worth remarking that using a null-bias between B and C provides no additional information for T_e, V_{gp}, and n, i.e., their probability distributions remain the same, and are then marginalized to calculate the probability distribution for the potential inhomogeneities (δV_1 and δV_2) sensed by the different electrodes for the different axial positions. This process is done for 80 different locations along the z axis. These probability distributions are then interpolated to obtain intermediate values and are introduced as prior probabilities in the main analysis of the time series corresponding to measurements with an applied bias V_{BC} of 30 V.

B. Time–frequency analysis

The analysis detailed in Sec. III A returns, as an output, the instantaneous plasma properties measured during the probe motion in terms of the most probable value and standard deviation of the probability distribution.

To study the frequency content of the plasma while the probe moved, a time–frequency analysis using wavelets was performed on the most probable properties signals. The analysis was configured to use analytic Morlet wavelets,[36] which are a family of analytic functions well-suited for the analysis of signals with time-varying amplitude and frequency. The adoption of a continuous wavelet transform of the properties' signal, together with the knowledge of the probe law of motion, allows to reconstruct the frequency content as a function of axial position. In turn, this gives insight into the structure of the breathing mode wave by showing the coherence (or potential dispersion) of the spectral content of the signals in the investigated domain. Moreover, by studying the phase shift in the wavelet cross-spectrum between the discharge current and the plasma properties, we can extrapolate the phase velocity and direction of the density, potential, and temperature wave during the breathing mode cycle.

It is important to note that, even though the probe is moving, the frequency scale of the arm motion is of the order of 1 Hz, and that of the plasma phenomena under analysis are of the order of tens of kHz. As a consequence, no correction is needed to consider the frequency Doppler shift caused by the probe movement. Nevertheless, to confirm the validity of this assumption, the wavelet analysis was repeated on

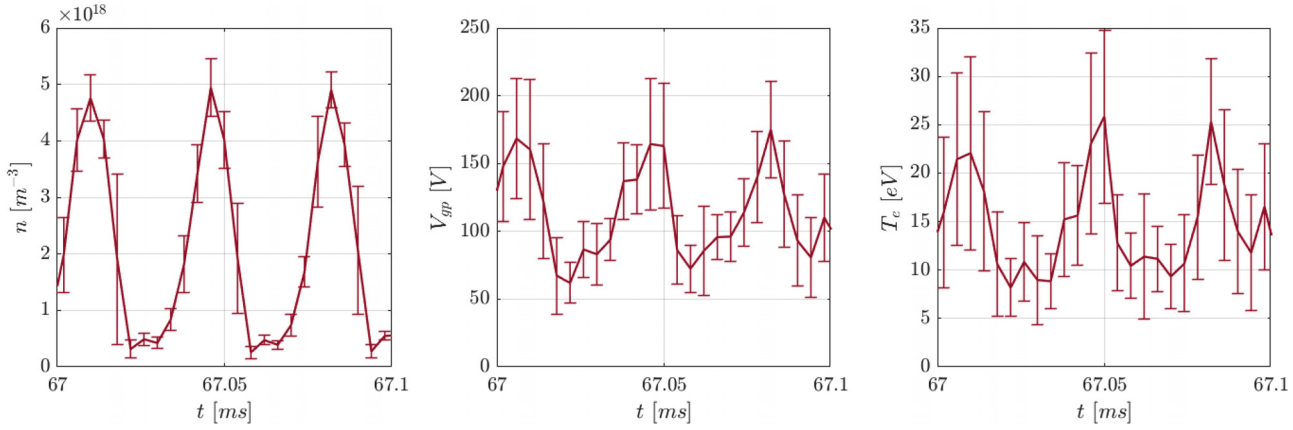

FIG. 6. Plasma parameters results with 1-σ standard deviation error bars for position z_1.

data acquired while the probe was moving away from the thruster, showing no changes in the frequency content of the signal.

C. Plasma global mode reconstruction

The plasma properties' profiles, and the probe law of motion can also be used to reconstruct the full z–t plane evolution of the plasma. This type of reconstruction was implemented by Lobbia *et al.* in Ref. 24 for the far plume of the thruster applying an averaged transfer function between discharge current and plasma properties measured on a 2D matrix of points. A similar processing technique was also applied to LIF measurements of the ion velocity, as presented in Ref. 23. The cited work used a reference discharge current signal as an input for the transfer function which modeled the whole domain. As stated by Lobbia *et al.*, this method requires large amounts of data to obtain a reliable averaged transfer function. Moreover, this approach loses accuracy in the near plume and in the vicinity of the channel exit plane, as the oscillations present a largely nonlinear behavior. For these reasons, a different approach is proposed.

Since the probe is measuring while moving, unlike the measurements in Ref. 24, the plasma properties data obtained with the fast diving probe are separated in both space and time. Therefore, it becomes necessary to shift the measured plasma properties in time so that the oscillations in the whole space domain evolve simultaneously, without losing the information on the phase shift of the signals at different locations. In the following, the method used to achieve spatiotemporal merging of the measured data is presented, together with the main assumptions adopted.

First, the signal is divided into subdomains of 200 samples. The selected subdomain size, corresponding to 0.8 ms, is short enough to neglect the displacement of the probe and consider it to be in a fixed position while the plasma evolves, as it displaces less than 1.3 mm in the furthermost region, where plasma has small gradients, and less than 0.6 mm close to the channel exit, where the gradients become larger. Moreover, the subdomains are long enough to assure that a significant number of breathing mode cycles are contained within each of them. The reference axial position for each subdomain is taken as the average of the position of the 200 points.

When time-shifting the signals, it is important to conserve the relative phase between the oscillations at different spatial locations, so the signal of the discharge current is used as a reference. Given the non-linearity of the plasma processes in the channel, the discharge current undergoes a small but non-negligible frequency modulation, with a 3 dB bandwidth of the signal of approximately 900 Hz, so the time separating two consecutive peaks is not perfectly constant. As a consequence, an optimization-based process is used to properly select and coordinate the signals between different axial locations.

The process starts by selecting, as a reference signal, a segment of the discharge current measurement containing an integer number of peaks, seven in the present analysis. Then, for each subdomain, an optimization process is followed to find the time shift that minimizes the sum of the distances between the peaks of the reference current signal and the peaks in the current signal corresponding to the subdomains to be shifted. Since we are dealing with an optimization in a discrete time domain, two or more different time shifts can yield the same result. In this case, the current signals are compared to the reference current signal, and the one that minimizes the euclidean norm of the signals' difference is selected. As a result, the segment of the subdomain which contains the seven best matching current peaks is conserved, and the data outside of it are discarded. Finally, once all the subdomains are time-shifted taking the discharge current as a reference, the resulting plasma signals are interpolated and plotted on a z–t surface, yielding a simultaneous picture of the plasma oscillations on the whole investigated domain.

IV. RESULTS AND DISCUSSION

The method described in Secs. II and III was used to characterize the properties of the plasma oscillations on the channel centerline of the HT5k DM2 firing at the operating point detailed in Table I. Figure 7 reports the discharge current raw signal measured with the oscilloscope for this operating condition during the probe insertion. The plot shows the signal as a function of the axial position of the probe tip relative to the thruster exit plane. It can be observed that, when the probe comes in proximity of the exit plane of the thruster, a significant increase in the average value of the discharge current is recorded, with a simultaneous decrease in the signal oscillation amplitude. This is symptomatic of the perturbation imposed on the thruster characteristics when the probe reaches the high azimuthal current and temperature regions. A possible explanation of this phenomenon is related to the secondary electrons emitted by the probe insulating material when exposed to the high temperature plasma.[12,14] This implies that the gathered data can be considered quantitatively representative of the thruster unperturbed behavior only starting from 2 mm downstream of the channel exit plane, corresponding to the position z_1 of Fig. 3. The results obtained inside the thruster channel are retained for completeness but should only be considered for qualitative considerations on the plasma behavior.

The discharge current shows oscillations with an amplitude of the order of the average current value. Figure 8 reports the power spectral density (PSD) of the discharge current signal of Fig. 7. Due to the comparatively low oscillatory component of the perturbed portion of the signal, the power spectral density of the unperturbed discharge

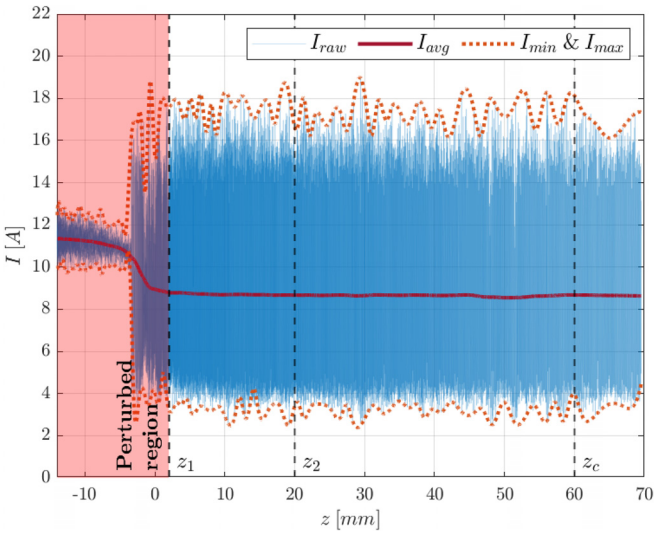

FIG. 7. Discharge current data during probe insertion vs axial position of the probe tip (referred to the channel exit plane).

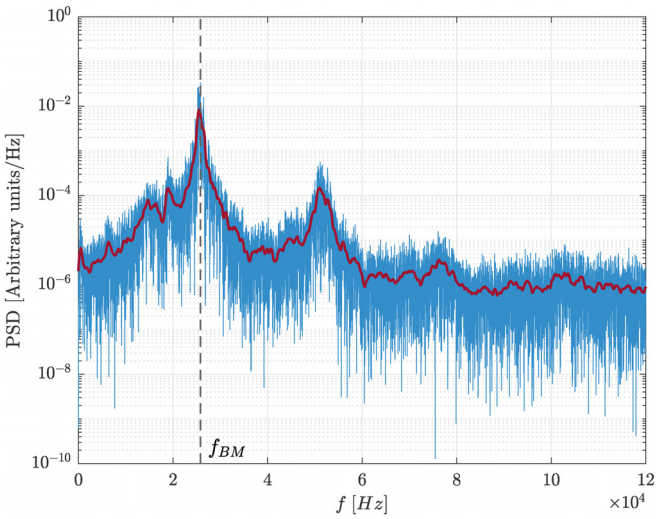

FIG. 8. Power spectral density of the full discharge current signal showing a clear dominant frequency with successive harmonics.

current signal presents the same features as the one of the complete signal and, thus, only the latter is reported. It is apparent how a clearly dominant frequency component exists for 25.8 kHz, with a secondary peak at the second harmonic frequency. These characteristics indicate that the thruster is operating in the global mode (as discussed by Ref. 3) with large amplitude longitudinal oscillations and a very clearly established breathing mode periodic cycle. The frequency corresponding to the peak in the current signal PSD is defined as the breathing mode frequency (f_{BM}) and referred to as such in the following.

The results of the post-processing of the probe data along its motion, in terms of plasma density, potential, and electron temperature are reported in Fig. 9. The time-averaged profiles are consistent with previous experimental efforts.[14] Density, potential, and temperature all increase from the far plume to the channel, with the plasma density reaching an average value of about 2×10^{18} at the channel exit section. The potential profile has strong gradients in the high magnetic field region close to the channel exit, and then plateaus in the channel to a value close to the applied discharge voltage of 300 V. The electron temperature profile peaks at about 20 eV in the high magnetic field region and then drops to low values inside the channel, due to ionization and wall energy losses. As depicted in Fig. 9, the density profile presents very high oscillations amplitude, of the order of the mean value, while the potential and temperature show relatively smaller oscillations, with the maximum values concentrated in the high magnetic field region of the thruster. The characteristics of the oscillations are investigated in greater detail for the three axial locations of interest z_1, z_2, and z_c discussed in Sec. II B and depicted in Fig. 3. The quantitative results for the oscillations reconstructed in these three regions are reported in Table II.

The power spectral density graph of the plasma density, potential, and temperature signals have very similar features to the one of the discharge current of Fig. 8. All three properties show a concentrated frequency content around the breathing mode frequency, indicative of the global nature of the phenomenon.

A. Time–frequency analysis

In order to better understand the dynamics of the breathing mode and its global nature, a time–frequency analysis of the plasma properties signal was performed, as detailed in Sec. III B. Knowing the law of motion of the probe, the analysis then becomes space–frequency, reporting the characteristics of the spectrum of the signal as a function of axial position. Figure 10 presents the magnitude scalogram[36] obtained from the 1D coherent wavelet transform for the plasma density signal. For what concerns the magnitude plots, the results for potential and temperature present very similar features and, thus, only the density results are discussed. It is observed that the breathing mode frequency, and its harmonics, not only is the dominant frequency of the overall signal, but it is the dominant frequency at every instant during the probe motion. Excluding the regions were the probe strongly perturbs the plasma flow, the frequency content distribution of the plasma oscillations does not

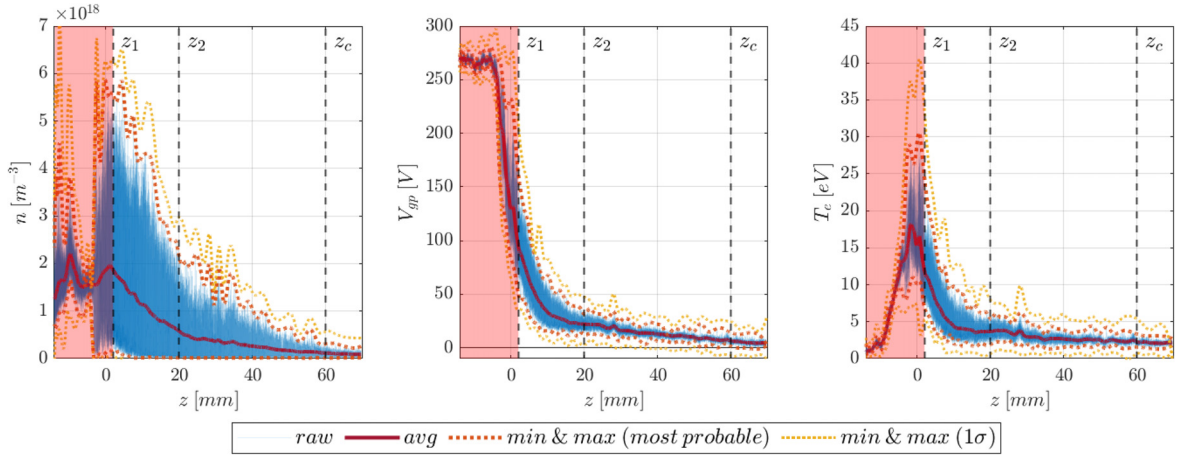

FIG. 9. Full dataset for the three plasma properties as a function of axial location relative to the thruster exit plane: (left) plasma density; (middle) plasma potential; and (right) electron temperature.

TABLE II. Oscillation characteristics in relevant axial positions.

		z_1	z_2	z_c
$n_{max\,(1\sigma)}$		63.10	29.74	5.76
n_{max}		55.71	21.39	3.13
$\mathbf{n_{avg}}$	$(10^{17}/\mathrm{m}^3)$	18.67	5.76	1.18
n_{min}		1.33	0.19	0.14
$n_{min\,(1\sigma)}$		0.66	0.00[a]	0.00[a]
$V_{gp\,max\,(1\sigma)}$		208.96	47.36	24.40
$V_{gp\,max}$		161.47	31.28	14.21
$\mathbf{V_{gp\,avg}}$	(V)	95.06	22.09	6.44
$V_{gp\,min}$		50.47	13.15	1.32
$V_{gp\,min\,(1\sigma)}$		35.64	3.37	−7.47
$T_{e\,max\,(1\sigma)}$		33.51	7.88	5.34
$T_{e\,max}$		24.39	5.34	3.29
$\mathbf{T_{e\,avg}}$	(eV)	11.84	3.68	2.26
$T_{e\,min}$		6.88	1.91	1.56
$T_{e\,min\,(1\sigma)}$		5.29	0.70	0.68

[a]Truncated at zero for physical meaningfulness.

change with the axial position and breathing oscillations observed in the discharge current signal correspond to coherent waves in the plasma domain with no frequency dispersion.

Additional detail on the wave dynamics can be gathered from the space–frequency wavelet analysis by considering the phase information. Assuming the discharge current signal as the phase reference, the wavelet cross-spectrum phase between any plasma property and the simultaneous discharge current signal returns the phase shift between the property signal and the reference as a function of frequency and axial location. By limiting the analysis at the breathing frequency component of all profiles, this analysis details how the breathing mode wave shifts in phase with respect to the discharge current as a function of position for all three plasma properties under investigation. The results are displayed in Fig. 11 both in terms of raw data and filtered profiles.

It is apparent how the trend is opposite between the density wave and the other two properties in the near plume. Moving further downstream from the channel exit, the relative phase between the density breathing mode frequency component and the discharge current increases, while the same value decreases for the temperature and potential. This suggests that, for the operating condition under investigation, while the density wave linked to the breathing mode is a coherent wave with a phase velocity directed outward along the channel centerline, the peaks of temperature and potential breathing mode waves seem to move from the plume toward the thruster channel. Another interesting feature is that all curves tend to low phase shifts when moving toward the channel, indicating that closer to the acceleration zone of the thruster the oscillations of all plasma properties tend to be in-phase with the current oscillations. Finally, the temperature and potential cross-spectrum phase graph show a global minimum in the axial position corresponding to the cathode line (z_c). This is more evident for the temperature profile, while the potential keeps an almost constant phase in the final part of the domain. While the phase profiles are significantly more disturbed in that region due to the low coherence of the signals and generally high signal-to-noise ratio, this seems to suggest that potential and temperature waves originate from the cathode and have a phase velocity in both directions: toward the channel, where the waves interact with the breathing mode dynamics, and outward, toward the far plume, lagging behind the density wave.

The availability of the phase shift between a property and a reference signal, together with the knowledge of the period of the wave, allow to know the time shift of the wave between two different axial locations. Knowing the spatial distance between the two points also allows to estimate the phase velocity of the coherent wave. Performing this analysis on the plasma density signal between z_1 and z_c, we obtained an average propagation speed of 15 050 m/s which is, as

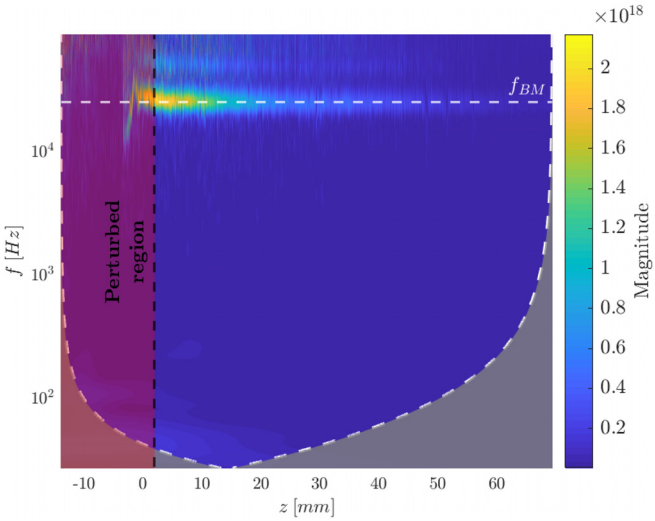

FIG. 10. Magnitude scalogram of the 1D coherent wavelet transform of the plasma density profile.

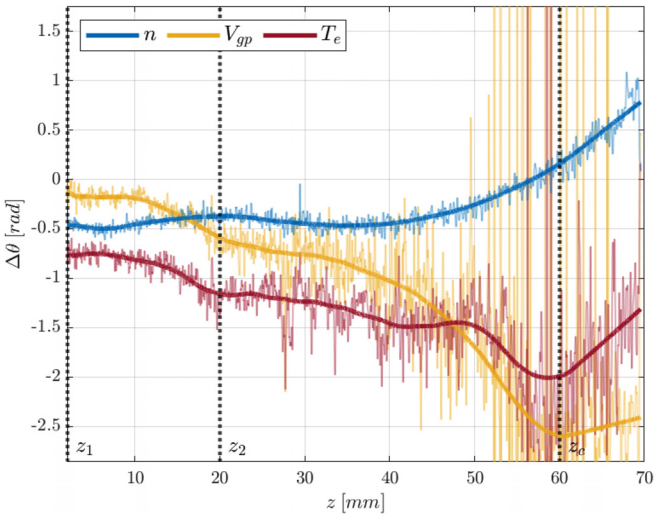

FIG. 11. Phase shift of the f_{BM} component of the wavelet cross-spectrum between plasma properties and discharge current as a function of axial location.

expected, of the same order of the electrostatic speed of a xenon ion accelerated through the discharge potential drop. Similar findings in terms of the breathing mode density wave propagation speed were found by other authors.[27] Figure 11 also shows that the density fluctuations appear to occur almost simultaneously in the first 40 mm outside the acceleration channel and their phase velocity significantly slows down near the cathode coupling region. Notably, we observe that the phase shift between density and current oscillations crosses zero, i.e., perfectly in phase, in the cathode coupling region, in close proximity to the axial location z_c.

While the density wave result is relatively straightforward to understand when associated with the accelerated ions as carriers, the phase shift for temperature and potential waves is the outcome of the complex near plume dynamic of the plasma, combining the transport linked with the flux of electrons emitted from the cathode with the effect induced by the outbound plasma density wave. If we perform the analysis of the phase shift for the temperature and potential signals, we obtain an average value of −3790 m/s for the phase velocity of the potential wave and −7580 m/s for the temperature wave. The two waves have an almost constant phase shift between each other of 0.5 rad in the first 40 mm outside the acceleration channel, whereas near the cathode line, the temperature signal has a variation of phase, that is, approximately half that of the potential. Finally, we notice that in the plume the phase offset between the plasma density and potential is the maximum and tends to π, whereas it reduces almost to zero at the exit of the acceleration channel. The interaction between the different processes highlighted before and their link with electron mobility and breathing mode oscillations will be the subject of future investigations.

B. Reconstruction of global modes

Finally, the global mode reconstruction technique discussed in Sec. III C was employed to obtain spatiotemporal merging of all available data and reconstruct the plasma oscillations on the full z–t plane. The final result of the analysis is presented in Fig. 12. This gives a striking depiction of the effect of breathing mode on the plasma fields from the plume up to the thruster channel. These results show the realization of the breathing mode as a non-dispersive periodic pulse of density being ejected out of the thruster, coupled with the same frequency ripples of potential and temperature in the high magnetic field region of the thruster. Particularly, it is apparent from the reconstructed potential profile that the position and extent of the acceleration region of the thruster evolve during the breathing cycle, alternating phases when most of the potential drop occurs inside the channel to phases when the acceleration region protrudes in the near plume. As a matter of fact, approximately 54% (161 V) of the applied discharge voltage drop of 300 V occurs downstream of the z_1 location at peak phases, while only approximately 17% (50 V) occurs during the opposing phase. This is coherent with the results obtained by other authors on the acceleration region dynamics.[23]

Observe that, on this scale, the propagation speed of the wave discussed in the previous chapter is too high to be resolved and the oscillations appear as instantaneously materializing on the whole z axis.

V. CONCLUSIONS

The present work described a novel diagnostic setup and data processing technique to investigate the longitudinal plasma oscillations in the plume and channel region of Hall thrusters. The adoption of a triple Langmuir probe allows for instantaneous measurements of the plasma density, potential, and electron temperature, avoiding the need for time-consuming potential sweeps, typical of single probes. Thanks to this property, the probe was installed on a rapidly moving arm that

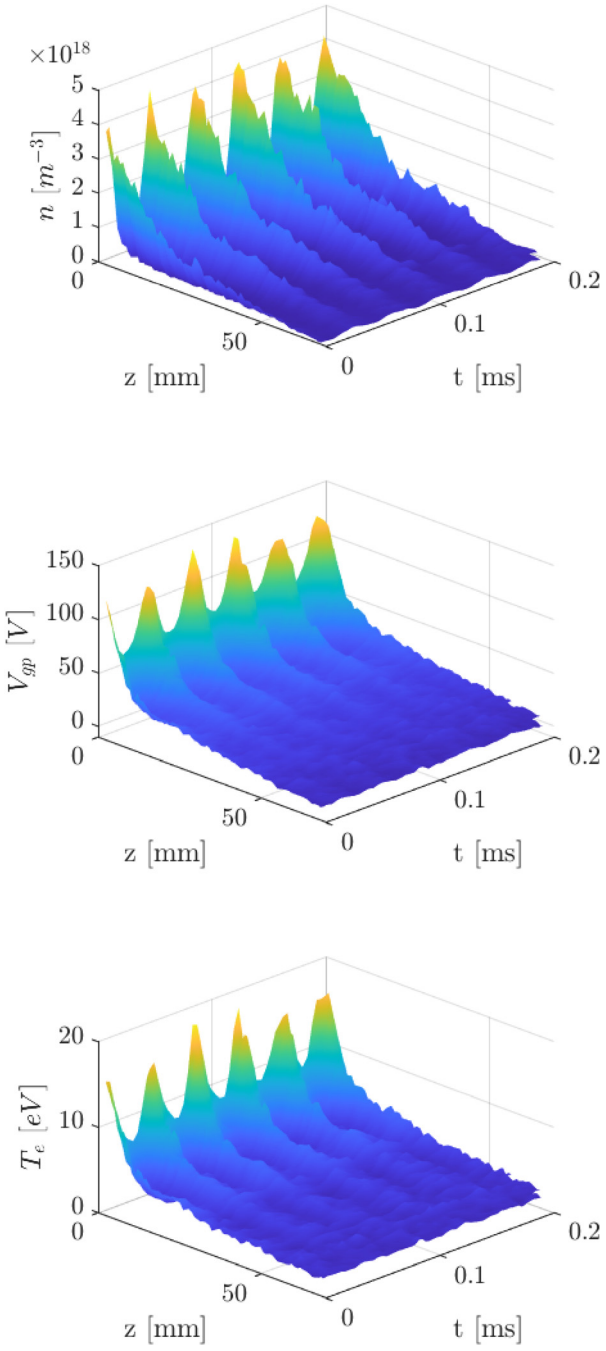

FIG. 12. Global reconstruction for $z > z_1$ of: (top) plasma density oscillations; (middle) plasma potential oscillations; and (bottom) electron temperature oscillations.

injects and removes the diagnostic tool from the high density and temperature plasma region in 0.2 s. The analogue probe signal was acquired through a 120 kHz-bandwidth electronic box and then sampled at 5 MHz with a Tektronix DPO4104 digital oscilloscope. The data were then processed with a Bayesian regression analysis coupled with a parameterization of the Laframboise sheath theory to obtain the instantaneous values of the three plasma properties. The effectiveness of this diagnostic system to gather information on the breathing mode oscillations of Hall thrusters was then demonstrated in an experimental campaign carried out on a 5 kW-class thruster, SITAEL's HT5k DM2. The results showed large oscillations of the plasma properties at the same frequency of the discharge current oscillations, typical of the breathing mode. The density showed particularly large oscillations on the whole domain, and all three properties had the peak of oscillation amplitude in the high magnetic field region of the thruster. A time–frequency analysis, based on wavelets, highlighted the coherent and non-dispersive structure of the longitudinal waves. Moreover, the wavelet cross-spectrum phase of the plasma properties with the discharge current at the breathing mode frequency gave information on the waves' phase speed. The results showed how peaks of the density wave propagate outward with a speed of the order of 15 km/s, while the potential and temperature waves seem to initiate at the cathode coupling region and have phase velocities directed toward the channel. Finally, we presented a spatiotemporal merging technique for all the available data, allowing to visualize simultaneously the breathing mode oscillations on all plasma properties on the whole domain.

The information produced gave a clear picture of the breathing mode as a global coherent and periodic plasma structure evolving along the plasma domain. This diagnostic system, and refined data processing technique, has demonstrated that with a single 0.2 s probe dive in the plasma region, it can produce a remarkable amount of quantitative information on the plasma dynamics in the thruster near plume. Even with some limitations, specifically concerning the probe perturbation when entering the channel, the same setup can be used to investigate multiple thruster configurations and operating points to gather valuable insight on the effect of the breathing mode on the plasma properties and to support the optimization of the thruster oscillatory behavior.

ACKNOWLEDGMENTS

The authors wish to express their gratitude to Ugo Cesari, Nicola Giusti, Luca Pieri, Stefano Caneschi, and Carlo Tellini for their valuable assistance in preparing and performing the experimental campaign. Fruitful discussion with Professor Fabrizio Paganucci is gratefully acknowledged. The work described in this paper has been partially funded by the European Space Agency in the framework of the Contract No. 4000113279/14/NL/KML "Low-Erosion Long-Life Hall-Effect Thruster." The view expressed herein can in no way be taken to reflect the official opinion of the European Space Agency.

APPENDIX: SELECTION OF NESTED SAMPLING ALGORITHM PARAMETERS

1. Sampling solution parameters

Bayesian computational methods based on Monte Carlo sampling, such as the nested sampling used in the present research have the disadvantage of being computationally expensive. The analysis of long time series of measured data made it necessary to perform an optimization of the solver parameters to achieve accurate solutions and avoid prohibitive computational times.

The nested sampling algorithm explores the domain by randomly selecting points in the domain (plasma parameters combinations in this case) and evaluating their likelihood. Then, it generates surfaces of constant likelihood and discards the least likely points.

The nested sampling implementation follows the one proposed in Ref. 35, which uses a Monte Carlo strategy to improve the search of new live points. The method has three tunable parameters, the first one being the number of live points N_{live} which are evaluated in each sampling step. The second parameter is the number of Monte Carlo iterations M_{MC} performed to select the new batch of live points. The most time-consuming step of the whole algorithm is the solution of the physical model, which is performed in each likelihood function evaluation, as a consequence, the solution time grows as the $N_{live} \cdot M_{MC}$ product.[35] Being a problem of five parameters, it has a rather low dimensionality, so three Monte Carlo iterations are acceptable. Finally, the third parameter is the tolerance for the evidence calculation. It is worth reminding that nested sampling is primarily a method for calculating the evidence in largely dimensional problems, which allows to accurately obtain the posterior probability of the parameters as a by-product. The iterations exploring the domain go on until little change in the evidence growth is observed.[32] In this case, the stopping criterion is that the change in the logarithm of the evidence in two successive steps is below the selected tolerance. A value of 10^{-3} was used for the tolerance to guarantee an acceptable level of convergence in the solution.

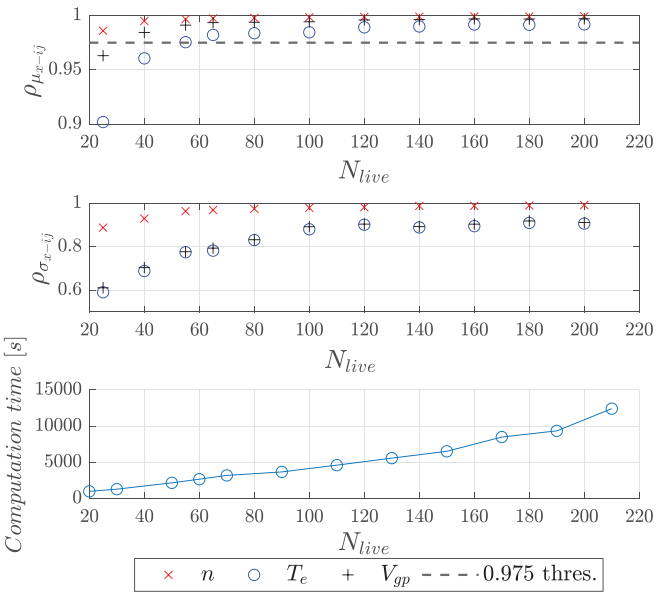

FIG. 13. Pearson correlation coefficient between consecutive solutions as a function of N_{live} for the mean values (top) and standard deviation (middle). Required computational time as a function of N_{live} (bottom).

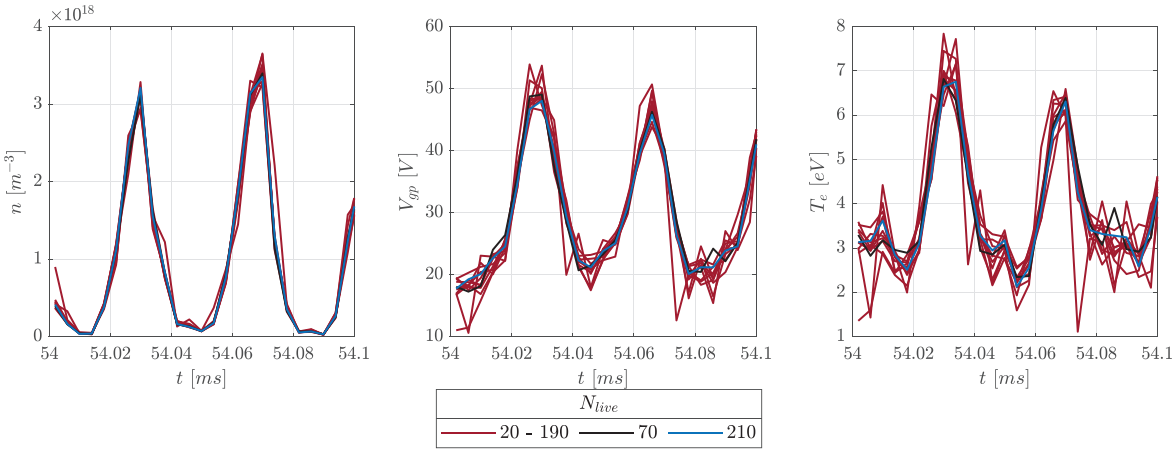

FIG. 14. Parameter solution example for different N_{live} values.

2. Sensitivity analysis

Having fixed the second and the third parameters, a parametric study varying N_{live} was made to assess the impact of the number of live points on the solution. To perform the study, the plasma parameter inference was repeated for different numbers of live points. The problem was solved for a sub-set of representative time frames of the data: 11 time frames of 200 μs (50 samples each), separated by 2 ms between 44 and 64.2 ms. The analyzed region corresponds to zones where the plasma has the highest oscillation amplitude. N_{live} was varied from 30 to 210 with a step of 20, and the solution results and computation time were recorded. Additionally, the cases with 20 and 60 live points were considered for a clearer representation of the error growth behavior. Finally, data were post-processed by calculating the Pearson correlation coefficient between the two successive solutions $N_{live} = i$ and $N_{live} = j$ of a given parameter x, both for the parameter mean $\rho_{\mu_{x-ij}}$ and the standard deviation $\rho_{\sigma_{x-ij}}$. The compared solutions are the time series of the mean values of the plasma parameters.

Figure 13 shows the calculated correlation coefficients and the computation time as a function of N_{live}. It is clear that the error is always smaller for the density than for the temperature and potential. This was expected, as the probe equations depend almost linearly on the density (except for the sheath expansion correction which depends weakly on the Debye length), while the dependence on temperature and potential is exponential. It is interesting to note that the convergence is much faster for the mean value than for the inference uncertainty, so the calculated mean value results obtained with less points can be considered reliably similar to the values obtained with more than 150 points. If we consider 0.975 as an acceptance threshold for all parameters, the use of 70 live points can be deemed acceptable.

Regarding computation time, it can be seen that, as expected, it grows almost linearly with the number of points. The depicted solution times correspond to a dataset of 550 points using a four core/8 thread i7-7700HQ CPU PC with 16 Gb of RAM and a solid state drive for the computation. For a complete dataset of 25 000 points, the times should be multiplied by $25\,000/550 \cong 45.5$, this implies that for 70 live points the total calculation time is of about 41 h, which was considered as an acceptable upper limit.

Figure 14 shows the results for plasma density, potential, and electron temperature for all the live point values. The blue curves represent the solutions when 210 live points were used, which can be considered as a reference value. The black curves are the solutions for 70 live points, the selected alternative, and the red curves represent the rest of the solutions. It is evident that the solutions for the density converge faster, as observed in Fig. 13, while for the electron temperature and plasma potential, the variation between the different results is larger. It can also be seen that the results using 70 live points are close to those using 210, further backing the decision of using 70 live points for the full solution.

DATA AVAILABILITY

The data that support the findings of this study are available from the corresponding author upon reasonable request.

REFERENCES

[1]J. P. Boeuf, "Tutorial: Physics and modeling of Hall thrusters," J. Appl. Phys. **121**, 011101 (2017).
[2]E. Y. Choueiri, "Plasma oscillations in Hall thrusters," Phys. Plasmas **8**, 1411 (2001).
[3]M. J. Sekerak, B. Longmier, A. Gallimore, W. Huang, H. Kamhawi, R. R. Hofer, B. Jorns, and J. E. Polk, "Mode transitions in magnetically shielded Hall effect thrusters," AIAA Paper No. 2014-3511, 2014.
[4]M. J. Sekerak, A. D. Gallimore, D. L. Brown, R. R. Hofer, and J. E. Polk, "Mode transitions in Hall-effect thrusters induced by variable magnetic field strength," J. Propul. Power **32**, 903–917 (2016).
[5]G. N. Tilinin, "High-frequency plasma waves in a Hall accelerator with an extended acceleration zone," Sov. Phys. Tech. Phys. **22**, 974 (1977).
[6]J. M. Fife, M. Martinez-Sanchez, and J. Szabo, "A numerical study of low-frequency discharge oscillations in Hall thrusters," in *Proceedings of the 33rd Joint Propulsion Conference and Exhibit* (American Institute of Aeronautics and Astronautics, Inc., 1997).
[7]J. P. Boeuf and L. Garrigues, "Low frequency oscillations in a stationary plasma thruster," J. Appl. Phys. **84**, 3541–3554 (1998).
[8]S. Barral and E. Ahedo, "Theoretical study of the breathing mode in Hall thrusters," AIAA Paper No. 2006-5172, 2006, Vol. 10, pp. 8117–8128.

[9]E. T. Dale and B. A. Jorns, "Two-zone Hall thruster breathing mode mechanism, Part I: Theory," in Proceedings of the 36th International Electric Propulsion Conference, 2019, Paper No. IEPC–2019–354.
[10]K. Hara, I. D. Boyd, M. J. Sekerak, and A. D. Gallimore, "Breathing mode in Hall effect thrusters," in Proceedings of the 30th ISTS, 34th IEPC and 6th NSAT, 2015, Paper No. IEPC–2015–293/ISTS–2015–b–283.
[11]O. Chapurin, A. Smolyakov, G. Hagelaar, J. P. Boeuf, and Y. Raitses, "Fluid and hybrid simulations of the ionization instabilities in Hall thruster," in Proceedings of the 36th International Electric Propulsion Conference, 2019, Paper No. IEPC–2019–762.
[12]J. M. Haas, A. D. Gallimore, K. McFall, and G. Spanjers, "Development of a high-speed, reciprocating electrostatic probe system for Hall thruster interrogation," Rev. Sci. Instrum. **71**, 4131 (2000).
[13]T. Andreussi, V. Giannetti, A. Leporini, M. M. Saravia, and M. Andrenucci, "Influence of the magnetic field configuration on the plasma flow in Hall thrusters," Plasma Phys. Controlled Fusion **60**, 014015 (2017).
[14]M. M. Saravia, A. Giacobbe, and T. Andreussi, "Bayesian analysis of triple Langmuir probe measurements for the characterization of Hall thruster plasmas," Rev. Sci. Instrum. **90**, 023502 (2019).
[15]T. Andreussi, M. Saravia, and M. Andrenucci, "Plasma characterization in Hall thrusters by Langmuir probes," J. Instrum. **14**, C05011 (2019).
[16]J. A. Linnell and A. D. Gallimore, "Internal plasma potential measurements of a Hall thruster using xenon and krypton propellant," Phys. Plasmas **13**, 093502 (2006).
[17]B. Jorns, D. M. Goebel, and R. R. Hofer, "Plasma perturbations in high-speed probing of Hall thruster discharge chambers: Quantification and mitigation," AIAA Paper No. 2015-4006, 2015.
[18]B. M. Reid, "The influence of neutral flow rate in the operation of Hall thrusters," Ph.D. thesis (University of Michigan, 2009).
[19]B. Vincent, S. Tsikata, S. Mazouffre, T. Minea, and J. Fils, "A compact new incoherent Thomson scattering diagnostic for low-temperature plasma studies," Plasma Sources Sci. Technol. **27**, 055002 (2018).
[20]S. Mazouffre, "Laser-induced fluorescence diagnostics of the cross-field discharge of Hall thrusters," Plasma Sources Sci. Technol. **22**, 013001 (2012).
[21]E. T. Dale and B. A. Jorns, "Two-zone Hall thruster breathing mode mechanism, Part II: Experiment," in Proceedings of the 36th International Electric Propulsion Conference, 2019, Paper No. IEPC–2019–352.
[22]E. T. Dale and B. A. Jorns, "Non-invasive time-resolved measurements of anomalous collision frequency in a Hall thruster," Phys. Plasmas **26**, 013516 (2019).
[23]V. H. Chaplin, R. B. Lobbia, A. Lopez Ortega, I. G. Mikellides, R. R. Hofer, J. E. Polk, and A. J. Friss, "Time-resolved ion velocity measurements in a high-power Hall thruster using laser-induced fluorescence with transfer function averaging," Appl. Phys. Lett. **116**, 234107 (2020).
[24]R. Lobbia and A. Gallimore, "A method of measuring transient plume properties," AIAA Paper No. 2008-4650, 2008.
[25]R. B. Lobbia and A. D. Gallimore, "Fusing spatially and temporally separated single-point turbulent plasma flow measurements into two-dimensional time-resolved visualizations," in Proceedings of the12th International Conference on Information Fusion, FUSION 2009, 2009, 678–685.
[26]R. B. Lobbia and A. D. Gallimore, "Two-dimensional time-resolved breathing mode plasma fluctuation variation with Hall thruster discharge settings," in Proceedings of the 31st International Electric Propulsion Conference, 2009, Paper No. IEPC–2009–106.
[27]R. B. Lobbia and A. D. Gallimore, "High-speed dual Langmuir probe," Rev. Sci. Instrum. **81**, 073503 (2010).
[28]V. Giannetti, E. Ferrato, A. Piragino, M. Reza, F. Faraji, M. Andrenucci, and T. Andreussi, "HT5k thruster unit development history, status and way forward," in Proceedings of the 36th International Electric Propulsion Conference, 2019, Paper No. IEPC–2019–878.
[29]S.-L. Chen and T. Sekiguchi, "Instantaneous direct-display system of plasma parameters by means of triple probe," J. Appl. Phys. **36**, 2363–2375 (1965).
[30]C. Ducci, S. Oslyak, D. Dignani, R. Albertoni, and M. Andrenucci, "HT100D performance evaluation and endurance test results," in Proceedings of the 33rd International Electric Propulsion Conference, 2013, Paper No. IEPC–2013–140.
[31]V. Dose, "Bayesian inference in physics: Case studies," Rep. Prog. Phys. **66**, 1421–1461 (2003).
[32]J. S. D. Sivia, *Data Analysis: A Bayesian Tutorial* (Oxford Science Publications, 2006).
[33]M. Mausbach, "Parametrization of the Laframboise theory for cylindrical Langmuir probe analysis," J. Vac. Sci. Technol., A **15**, 2923–2929 (1997).
[34]J. G. Laframboise, "Theory of spherical and cylindrical Langmuir probes in a collisionless Maxwellian plasma at rest," Technical Report No. 100 (University of Toronto Institute for Aerospace Studies, 1966).
[35]J. Veitch and A. Vecchio, "Bayesian coherent analysis of in-spiral gravitational wave signals with a detector network," Phys. Rev. D **81**, 062003 (2010).
[36]*Wavelets in Physics*, edited by J. C. van den Berg (Cambridge University Press, 1999).